Possible Gas-Phase Reactions of H_2/CH_4/Tetramethylsilane in Diamond/β-SiC Nanocomposite Film Deposition: An Ab-Initio Study

Y. L. Zhao,[†] R. Q. Zhang,*[,‡] Vadali. V. S. S. Srikanth,[§] and X. Jiang*[,§]

Institute of Material Science and Engineering, Ocean University of China, Qingdao, Shangdong 266100, China, Centre of Super-Diamond and Advanced Films (COSDAF) & Department of Physics and Materials Science, City University of Hong Kong, Hong Kong SAR, China, and Institute of Materials Engineering, University of Siegen, Paul-Bonatz-Str. 9-11, 57076 Siegen, Germany

Received: January 2, 2007; In Final Form: March 13, 2007

The Si−C bond breakings in tetramethylsilane (TMS) when interacting with H/H_2 and the successive H abstractions from SiH_4/CH_4 in the gas mixture of H_2/ CH_4/TMS were studied at the CCSD(T)/6-311+G**// MP2/6-31+G** level of theory. Their rate constants between 1500 and 2500 K were estimated using a conventional transition state theory. The results indicate that (i) it is mainly the H radical that causes the Si−C bond breaking in TMS, and (ii) the successive H abstractions from SiH_4 are much easier and faster than those from CH_4. At low temperatures the differences of rate constants among the four types of the reactions are large, but generally reduced at high temperatures. The reaction rates show no selectivity over the pressure as verified at $P = 0.00025$, 0.025, 1, and 100 atm, respectively. Our results could provide the following microscopic level understanding of reactions in the synthesis of diamond/β-SiC nanocomposite films. Although the Si content is smaller than that of C in the precursor gases, the gas mixture activated by microwave plasma technique could provide Si sources with a higher rate. The produced Si sources with excellent rigidity in sp^3 hybridization competitively occupy the space on the substrate together with C sources, resulting in the deposition of diamond/β-SiC nanocomposite films.

1. Introduction

To overcome the difficulties involved in diamond film adhesion to different substrates and also to avoid any catalytic effects,[1−9] Jiang et al.[10−13] have successfully synthesized diamond/β-SiC nanocomposite films that act as interlayers to diamond top layers on Si substrates which were pretreated with nanodiamond particles. The synthesis was realized by using a microwave plasma-assisted chemical vapor deposition (MWCVD) technique and a gas mixture of H_2, CH_4, and tetramethylsilane [$(CH_3)_4Si$, TMS] (99.3−99.7 vol % H, 0.3−0.7 vol % CH_4, and 0.007 vol % TMS) as the precursor. An interesting observation[10,12] is that a little TMS addition to the gas mixture can produce a β-SiC-rich nanocomposite film. For example,[12] it is reported that if the TMS concentration is increased from 0% to only about 0.05% in the feed gas, the films will change from a pure diamond to a pure β-SiC phase. It implies that the TMS concentration strongly affects the molar fraction of the diamond/β-SiC composite film although the volume of CH_4 and TMS is at a great disparity in the feed gas. It was proposed that there is a competition between the diamond and β-SiC crystallites to occupy selective spaces available on the substrate, which was verified by experimental observations.[13]

To achieve a microscopic level understanding and control of the synthesis, it is worth studying the gas-phase reactions in the gas mixtures of H_2, CH_4, and TMS. Since TMS has a relatively large molecular weight and also is the only initial source to provide Si species, our focus at first would be on the resultant products from TMS, that is, on the Si−C bond breaking chemical reactions. Among the previous experimental reports[14−18] on the decomposition products of TMS, Seo et al.[14] produced 3C−SiC(111) films on Si substrates from TMS, employing a rapid thermal CVD technique above 1000 °C. They suggested that TMS is almost completely decomposed into H and Si atoms and hydrocarbon gases such as CH_4, C_2H_2, and C_2H_4 at the SiC growth temperature. Herlin et al.[15] studied the growth mechanism of SiC on a graphite susceptor in a low-pressure cold-wall reactor. They found that dissociation of TMS releases H atoms, various Si-containing species [$(CH_3)_3Si$, $(CH_3)_2SiCH_2$, etc.] and hydrocarbons. Jiang et al.[10−13] synthesized the composite films at the plasma temperature range of 1500−2500 K and well testified that TMS concentration really affects the molar fractions of diamond and β-SiC. Although they proposed the occurrence of gas-phase chemical reactions, the chemical species formed in the feed gas were not discussed in detail. Due to the discrepancy among the experiments, there has been no consistent conclusion about the products from TMS decomposition.

In addition to the experimental reports about the SiC growth mechanism and TMS decomposition, a number of molecular mechanic (MM) theoretical studies also exist.[19−22] For example, by performing thermodynamic calculations using the NASA CET89 program, Lee et al.[19] have proposed that C_2H_2 and SiH_n are the primary sources of C and Si depositions whereas the contribution from Si and CH_4 is very little; TMS could decompose at a high temperature as the total pressure increases. Henry et al.[20] have used TMS as the reactant and synthesized polycrystalline layers of β-SiC in a hot-walled reactor. By calculating the partial pressure of each possible product, they found a decreasing trend only in the case of Si and carbosilanes

* Corresponding authors. E-mail: aprqz@cityu.edu.hk (Dr. R. Q. Zhang); xin.jiang@uni-siegen.de (Prof. X. Jiang).
[†] Ocean University of China.
[‡] City University of Hong Kong.
[§] University of Siegen.

10.1021/jp070014s CCC: $37.00
Published on Web 04/19/2007

among the main components and byproducts of TMS pyrolysis reaction. The above-discussed investigations about the behavior of TMS in gas phase are all based on the MM theory, and the accuracy of such theoretical predictions is not very convincing. In this paper, quantum mechanical (QM) ab-initio simulations were used to explore the possible gas-phase microscopic reactions of H_2/CH_4/TMS in order to obtain more accurate potential energy surfaces and reaction heats. We aim at providing meaningful guidance to control the favorable experimental conditions so as to synthesize materials with desired properties.

2. Theoretical Approaches

Stationary points on the potential energy surface of the reaction system were fully optimized at the MP2/6-31+G** level of theory, followed by the calculation of harmonic vibration frequencies to confirm their nature as minima or first-order saddle points. For transition state (TS) structures, intrinsic reaction coordinate (IRC) calculations were performed to confirm if the TS structures really connect to the reactants and products. To accurately obtain total electronic energies, the structures determined at the MP2/6-31+G** level were used to calculate the single-point energy at the CCSD(T)/6-311+G** level (denoted as CCSD(T)/6-311+G**//MP2/6-31+G**). All calculations were performed using the *Gaussian 03* package.[23]

The determined total energies and frequencies were used to estimate the reaction rate constants. According to a conventional transition state theory (TST),[24−26] the rate constant can be expressed as

$$k = A \exp\left(-\frac{\Delta E^{\ddagger}}{RT}\right)$$

where the Arrhenius pre-exponential factor, A, is given by

$$A = \frac{k_B T e^2}{h} \frac{RT}{P_0} \exp\left(\frac{\Delta S^{\ddagger}}{R}\right)$$

where R, k_B, and h are the gas constant, Boltzmann constant, and Planck constant, respectively. P_0 is the standard pressure, being 101325 Pa. T is the environmental temperature. The activation energy, $\Delta E^{\ddagger}$, can be estimated by calculating the total energy difference between the transition state and the reactants. Similarly, the activation entropy, $\Delta S^{\ddagger}$, can be obtained by calculating the entropy difference between the transition state and the reactants. Here, the entropies are obtained according to a statistical thermodynamic approach. The temperature range for the reaction rate constant calculations is chosen to be 1500−2500 K according to the experiments.[10−13]

3. Results and Discussion

3.1. Activation Energies (ΔE_a) and Reaction Heats (ΔH_f).

3.1.1. Sequential Departures of CH_3 from TMS Assisted by H.

In the plasma environment of TMS (small percent), CH_4 (small percent) and H_2 (large percent) at 1500−2500 K, there is a definite existence of abundant H radicals produced from the thermal dissociation of H_2. To reveal the possible species produced from TMS in such an atmosphere, the Si−C bond breakings in TMS assisted by H radicals are designed as the following reaction equations:

$$(CH_3)_4Si + H \rightarrow (CH_3)_3Si + CH_4 \quad (1)$$

$$(CH_3)_3SiH + H \rightarrow (CH_3)_2SiH + CH_4 \quad (2)$$

$$(CH_3)_2SiH_2 + H \rightarrow (CH_3)SiH_2 + CH_4 \quad (3)$$

$$(CH_3)SiH_3 + H \rightarrow SiH_3 + CH_4 \quad (4)$$

Reactions (R) (1)−(4) depict the successive processes of CH_3 radicals escaped from TMS one by one with the assistance of H radical. Figure 1a−d illustrates the configurations of the products. As shown in Figure 1a, the Si atom still remains in the sp^3 configuration after one CH_3 abstraction from TMS as in R (1). Simultaneously, a hydrogen radical in the gas atmosphere easily attaches itself on the empty space of Si, resulting in the saturated $(CH_3)_3SiH$. In R (2), CH_3 abstraction from $(CH_3)_3SiH$ also produces an sp^3-like $(CH_3)_2SiH$, as shown in Figure 1b. Similarly, the resultant products of R (3)−(4) are also three-dimensional, as shown in Figure 1c−d, respectively. Under the continuous attack by H radicals, the four Si−C bonds of TMS will break at a certain time (sooner or later) and finally produce one SiH_3 radical and four CH_4 molecules, assuming R (1)−(4) could proceed smoothly.

At the CCSD(T)/6-311+G**//MP2/6-31+G** level of theory, structure optimizations, TS searches, and IRC confirmations were carried out for the four reactions discussed above. Figure 2a−d presents the optimized TS structures, which are denoted as TS1, TS2, TS3, and TS4 for R (1)−(4), respectively. All these TS structures look similar. In TS1−TS4, the breaking Si−C bond is elongated to 2.103, 2.096, 2.080, and 2.113 Å, respectively, considerably longer than the 1.886 Å of a regular Si−C single-bond length in TMS. The obtained TS structures all indicate that the outer H radical is gradually approaching the C atom and subsequently pulling the CH_3 out of the matrix. Accordingly, the departure of a CH_3 radical from TMS finally results with the assistance of an H radical. Table 1 lists the activation energy (ΔE_a) and reaction heat (ΔH_f) values of R (1)−(4). The ΔE_a values of TS1−TS4 are 43.51, 43.32, 43.13, and 44.35 kcal/mol, respectively. They are all small. The ΔH_f values are −12.35, −13.60, −15.16, and −16.93 kcal/mol, respectively, revealing exothermic reactions. Hence, the plasma-activated TMS favors the decomposition into CH_4 and $(CH_3)_{3-n}SiH_n$ ($n = 0-3$) species.

3.1.2. Sequential Departures of CH_3 from TMS Assisted by H_2.

Given the abundant H_2 in the gas mixture, their reactions with TMS are thus considered. Reactions (5)−(8) describe the sequential processes of TMS interactions with H_2 that involve successive abstractions of the methyl radical from the TMS and a subsequent leaving of a H atom.

$$(CH_3)_4Si + H_2 \rightarrow (CH_3)_3SiH + CH_4 \quad (5)$$

$$(CH_3)_3SiH + H_2 \rightarrow (CH_3)_2SiH_2 + CH_4 \quad (6)$$

$$(CH_3)_2SiH_2 + H_2 \rightarrow (CH_3)SiH_3 + CH_4 \quad (7)$$

$$(CH_3)SiH_3 + H_2 \rightarrow SiH_4 + CH_4 \quad (8)$$

The optimized transition state structures TS5, TS6, TS7, and TS8, shown in Figure 2e−h, respectively, are similar to each other. For instance, in TS5, the Si, C, and two H atoms from H_2 form a planar four-membered ring, as shown in Figure 2 e. The breaking Si−C bond and H−H bond are elongated by 19.03% and 48.77%, respectively, much longer than the respective regular Si−C and H−H bond lengths of 1.886 and 0.734 Å. Similarly, the forming C−H bond and Si−H bond

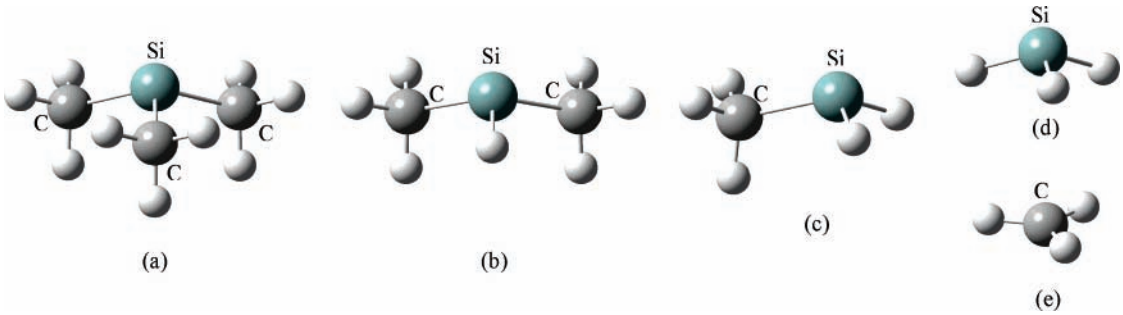

Figure 1. Geometrical structures of products from the reactions of TMS with H radicals (a) $(CH_3)_3Si$, (b) $(CH_3)_2SiH$, (c) $(CH_3)SiH_2$, (d) SiH_3 and product of $CH_4 + H \rightarrow CH_3 + H_2$, and (e) CH_3.

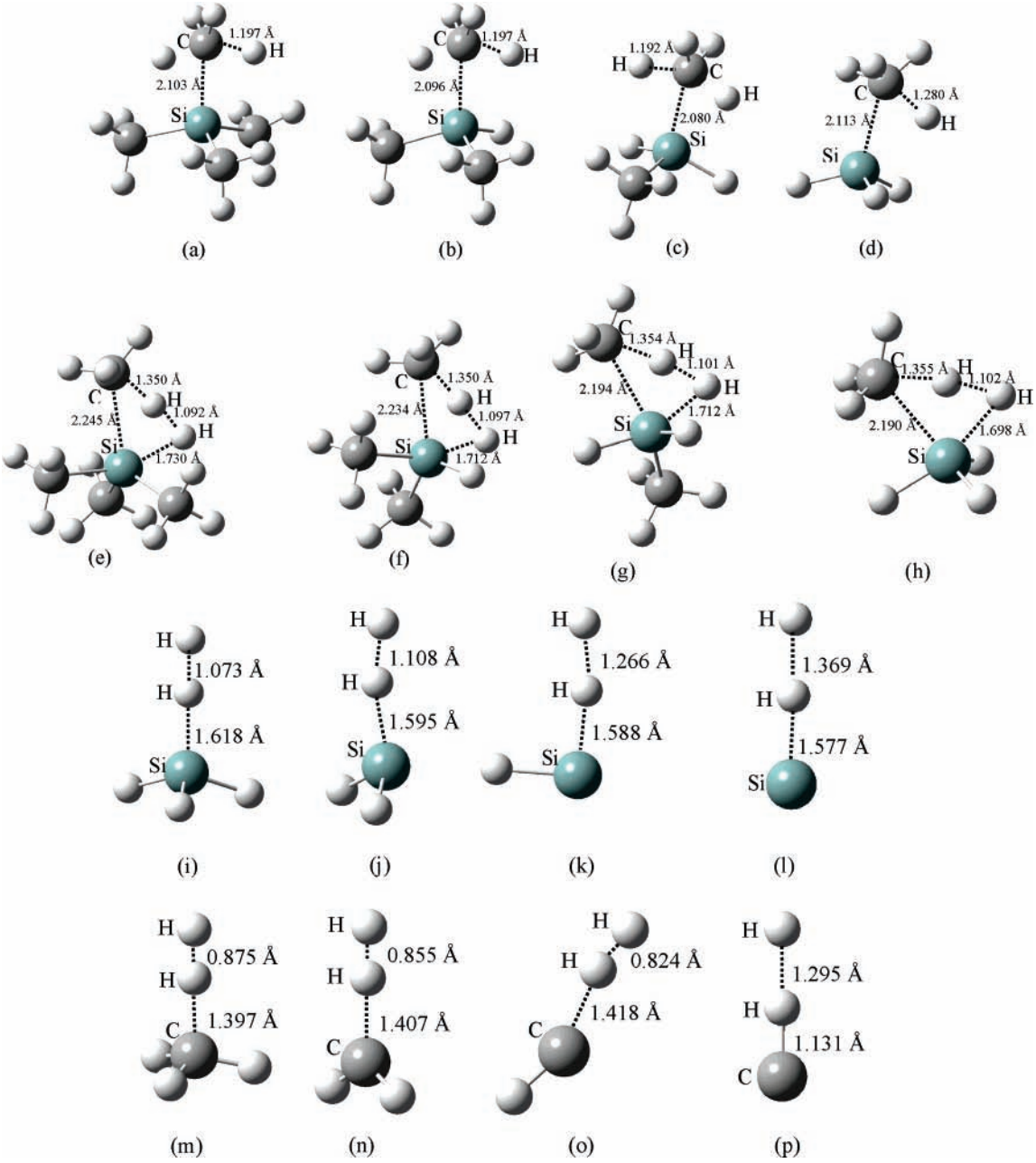

Figure 2. Transition state (TS) structures of R (1)−(4): (a) TS1, (b) TS2, (c) TS3, and (d) TS4; R (5)−(8): (e) TS5, (f) TS6, (g) TS7, and (h) TS8; R (9)−(12): (i) TS9, (j) TS10, (k) TS11, and (l) TS12; and R (13)−(16): (m) TS13, (n) TS14, (o) TS15, and (p) TS16.

are longer than their equilibrium values of 1.086 and 1.473 Å by 24.31% and 17.45%, respectively. As a result, the H atom from H_2 gets attached to the methyl and then escape together from the matrix, and the other H atom occupies the vacant position on the Si atom. Finally, the R (5) in which the TMS reacts with H_2 produces a $(CH_3)_3SiH$ and a CH_4, and so do R (6)−(8), as shown in Figure 2f−h. For R (5)−(8), four methyls of TMS will leave from the matrix, resulting in the products of

TABLE 1: Relative Energies (kcal/mol, ZPE corrections are included) for Possible Reactions (R) in the Gas Mixture of H2/CH4/TMS at the CCSD(T)/6-311+G//MP2/6-31+G** Level of Theory**

reactions (R)	activation energies (ΔE_a) (kcal/mol)	reaction heat (ΔH_f) (kcal/mol)
(1) $(CH_3)_4Si + H \rightarrow (CH_3)_3Si + CH_4$	43.51	−12.35
(2) $(CH_3)_3SiH + H \rightarrow (CH_3)_2SiH + CH_4$	43.32	−13.60
(3) $(CH_3)_2SiH_2 + H \rightarrow (CH_3)SiH_2 + CH_4$	43.13	−15.16
(4) $(CH_3)SiH_3 + H \rightarrow SiH_3 + CH_4$	44.35	−16.93
(5) $(CH_3)_4Si + H_2 \rightarrow (CH_3)_3SiH + CH_4$	83.32	0.5785
(6) $(CH_3)_3SiH + H_2 \rightarrow (CH_3)_2SiH_2 + CH_4$	83.48	−0.006069
(7) $(CH_3)_2SiH_2 + H_2 \rightarrow (CH_3)SiH_3 + CH_4$	82.49	−0.7262
(8) $(CH_3)SiH_3 + H_2 \rightarrow SiH_4 + CH_4$	84.14	−1.586
(9) $SiH_4 + H \rightarrow SiH_3 + H_2$	6.092	−15.34
(10) $SiH_3 + H \rightarrow SiH_2 + H_2$	5.650	−35.73
(11) $SiH_2 + H \rightarrow SiH + H_2$	2.474	−30.64
(12) $SiH + H \rightarrow Si + H_2$	2.587	−36.38
(13) $CH_4 + H \rightarrow CH_3 + H_2$	14.66	−3.231
(14) $CH_3 + H \rightarrow CH_2 + H_2$	15.13	1.621
(15) $CH_2 + H \rightarrow CH + H_2$	17.22	−5.679
(16) $CH + H \rightarrow C + H_2$	9.496	−28.63

$(CH_3)_{4-n}SiH_n$ ($n = 1-4$) and CH_4. As shown in Table 1, the ΔE_a values for R (5)−(8) are 83.32, 83.48, 82.49, and 84.14 kcal/mol, with ΔH_f values being just 0.5785, −0.006069, −0.7262 and −1.586 kcal/mol, respectively. The ΔE_avalues for R (5) − (8) are about two times those of R (1)−(4) and ΔH_f values are nearly zero, both not thermodynamically and kinetically facilitating Si−C breakings. Accordingly, the Si−C bonds of TMS broken by H_2 molecules are more difficult than those by H radicals. Therefore, the H radicals play an important role in the gas-phase reactions in the plasma feed gas.

3.1.3. Successive H Abstractions on SiH_4 and CH_4.

As the H radicals may lead to Si−C bond breakings of TMS, the gas-phase reactions are both diverse and complicated at a high temperature. Some radical reactions are barrierless and probably reversible. It was even proposed that Si atoms of Si substrates would continuously diffuse out to the surface and then participate in the gas-phase reactions.[14,27−28] Regardless of other factors (temperature, pressure, etc.), the real situation in the experiment is that different TMS gas rates will actually produce different molar fractions of diamond/β-SiC composite films.[12] In this connection, though the gas-phase CH_4 concentration is a hundred times greater than that of TMS in each experiment, the C sources in the plasma cannot lead to the diamond deposition as the main product at higher concentrations of TMS. On this basis, it was previously concluded[13] that there must exist a vehement competition between the diamond- and β-SiC-forming species from the gas phase to occupy the suitable vacant spaces on the substrate.

Accordingly, the product from Si−C bond breakings of TMS could provide the Si sources like SiH_n ($n = 0-3$) with the continuous assistance of H radicals. Considering that C sources like CH_n($n = 0-3$) could also be created by the reactions of CH_4 with H, we now comparatively study the successive H abstractions on SiH_4 and CH_4. The R (9)−(16) representing these abstraction reactions are given in the following:

$$SiH_4 + H \rightarrow SiH_3 + H_2 \quad (9)$$

$$SiH_3 + H \rightarrow SiH_2 + H_2 \quad (10)$$

Reactions (9)−(12) show that SiH_4 could decompose into

$$SiH_2 + H \rightarrow SiH + H_2 \quad (11)$$

$$SiH + H \rightarrow Si + H_2 \quad (12)$$

$$CH_4 + H \rightarrow CH_3 + H_2 \quad (13)$$

$$CH_3 + H \rightarrow CH_2 + H_2 \quad (14)$$

$$CH_2 + H \rightarrow CH + H_2 \quad (15)$$

$$CH + H \rightarrow C + H_2 \quad (16)$$

SiH_3, SiH_2, SiH, and finally to a Si atom as the H atoms from silane are abstracted one by one by a foreign H radical, and so does the CH_4 into the products CH_n ($n = 0-3$) in R (13)−(16). It is noted that the SiH_3 remains as a good sp^3 hybridized structure, whereas the CH_3 changes to an sp^2 planar structure, as shown in Figure 1, parts d and e, respectively. Such a structural difference would lead to a difference in growth rate between that of diamond and β-SiC when the Si or C sources competitively get attached on the sp^3-like substrate. This is an intrinsic reason why little Si content could compete with rich C sources during the deposition. The TS structure parameters for R (9)−(16) are clearly shown in Figure 2i−p, denoted as TS9−TS16. Here, we do not give detailed descriptions for their geometries any more.

At the CCSD(T)/6-311+G**//MP2/6-31+G** level of theory, the ΔE_a and ΔH_f values for R (9)−(16) were obtained, respectively, as listed in Table 1. The involved radicals among reactants and products are, respectively, optimized at their lowest multiplicities in order to select the most stable energy. For high spin systems, the spin contaminations are found to be small. The ΔE_a values for R (9)−(12) are 6.092, 5.650, 2.474, and 2.587 kcal/mol, respectively. The ΔH_f values are −15.34, −35.73, −30.64, and −36.38 kcal/mol, respectively, all negative. Judging from the low ΔE_a and large exothermic ΔH_f values, we can conclude that there is a great possibility for the series of reactions on SiH_4 by H radicals to proceed. As for R (13)−(16), their ΔE_a values are 14.66, 15.13, 17.22, and 9.496 kcal/mol, respectively, relatively high. Furthermore, the ΔH_f values are not all negative, for example, 1.621 kcal/mol for R (14) . Therefore, from the viewpoint of thermodynamic study, we could conclude that the successive H abstractions on silane should be easier and quicker than those on methane.

3.2. Rate Constants.

To quantitatively study the gas-phase reactions, the rate constants are calculated according to the above formula using the conventional TST. As the experiments performed by Jiang et al.[10−13] were at a pressure of 25 mbar, we calculated rate constants, k, for R (1)−(16) at $P = 0.025$ atm. Figure 3

TABLE 2: Rate Constant Comparisons between Theory and Experiment

	theory			experiment		
reactions (R)	k ($dm^3\,mol^{-1}\,s^{-1}$)	T (K)	P (atm)	k ($dm^3\,mol^{-1}\,s^{-1}$)	T (K)	P (atm)
(13) $CH_4 + H \rightarrow CH_3 + H_2$	3.30×10^{10}	2000	1	1.64×10^{10} [29]	2000	1.58
(15) $CH_2 + H \rightarrow CH + H_2$	3.80×10^{9}	2000	1	8.00×10^{9} [31]	1450−2500	1.58

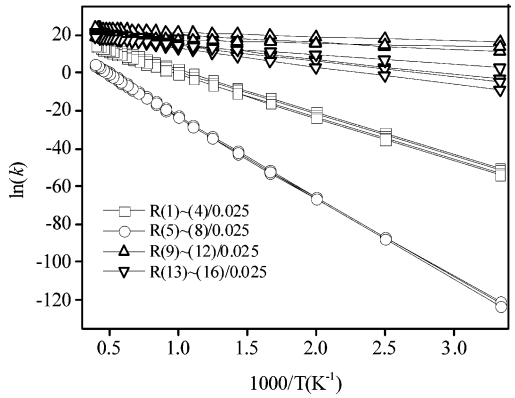

Figure 3. The calculated rate constants ($dm^3\ mol^{-1}\ s^{-1}$) of R (1)−(16) at the pressure of 0.025 atm.

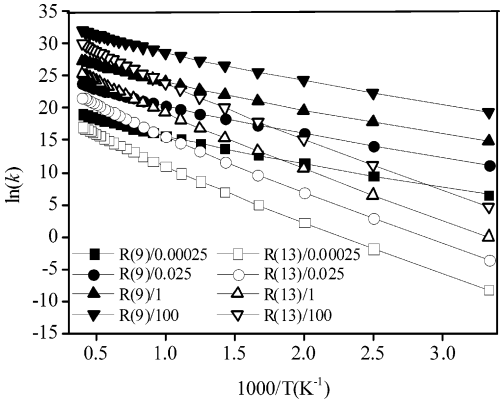

Figure 4. The calculated rate constants ($dm^3\ mol^{-1}\ s^{-1}$) of R (9) and R (13) at pressures of 0.00025, 0.025, 1, and 100 atm.

illustrates the ln k as a function of 1000/T. Obviously, in the temperature range from 1500 to 2500 K, the order of k should be $k_{R(9)-(12)} > k_{R(13)-(16)} > k_{R(1)-(4)} > k_{R(5)-(8)}$. Accordingly, the rate constants of R (9)−(12) are the highest, but those of R (5)−(8) are the lowest. Since the plasma temperature varies in the range of 1500−2500 K, we checked the rate constants at a middle value, $T = 2000$ K, at the pressure of 0.025 atm. The calculated rate constants for R (1)−(8) are 1.1×10^6, 3.1×10^5, 5.7×10^4, 8.9×10^4, 8.2×10^{-1}, 3.0×10^{-1}, 3.5×10^{-1}, and 4.7×10^{-1} $dm^3\ mol^{-1}\ s^{-1}$, respectively. From the 5−7 orders of magnitude difference between R (1)−(4) and R (5)−(8), it quantitatively proves again that it is the H radical but not H_2 that plays an important role in the gas-phase Si−C breaking reactions. Moreover, the rate constants for R (9)−(12) (1.0×10^{10}, 5.6×10^9, 9.5×10^9, and 1.3×10^8 $dm^3\ mol^{-1}\ s^{-1}$) are about 10−100 times greater than those for R (13)−(16) (8.4×10^8, 3.3×10^8, 9.6×10^7, and 5.7×10^7 $dm^3\ mol^{-1}\ s^{-1}$). Thus, it is also testified that the successive H abstractions from SiH_4 are easier and faster than those from CH_4. On the other hand, it is revealed that the degrees of sensitivity (S) to temperature for these four types of reaction constants follow $S_{R(9)-(12)} < S_{R(13)-(16)} < S_{R(1)-(4)} < S_{R(5)-(8)}$ because the k variation tendency is the mildest for R (9)−(12) but most abrupt for R (5)−(8) as the temperature increases. Accordingly, at a low-temperature range, the rate constants of R (9)−(12) are much larger than those of R (13)−(16), but both getting contiguous as T moves to the high range, so are the relationships between R (1)−(4) and R (5)−(8). These kinetic trends of the gas-phase reactions could provide clear temperature-selection guidance for experimentalists to control experimental conditions.

Furthermore, since R (9) and R (13) provide the vital species attached on the substrate, we investigated their rate-constant change with different pressures from 0.00025, 0.025, and 1 to 100 atm. As shown in Figure 4, the curves for the same reaction at different pressures look alike and are almost parallel to each other, they just have different absolute values. It implies that the rate constants of R (9) and R (13) could both increase uniformly as the pressure increases from 0.00025, 0.025, and 1 to 100 atm. Thus, the reaction rate has no special selectivity to any pressure. Also, we could have a clear observation that for R (9) or R (13) at each pressure, the curve is almost straight in the low-temperature range, whereas the curve slope gradually gets steeper at a high-temperature range. It means the reaction rates will have an accelerated variation with the increase of the temperature in a high range. The variation tendency of R (9) at pressures of 0.00025, 0.025, 1, and 100 atm are milder than those of R (13), in agreement with the trends shown in Figure 3.

To confirm the validity of our theoretical values, we compared the k values between theory and experiment. As shown in Table 2, the data from TST calculations are very close to the experimental ones, which were obtained at $P = 1200$ Torr and $T = 2000$ K. The theoretical values of R (13) and R (15) are in the same order of magnitude as those of experiments. Although the pressure in calculation (1 atm) is a little different from the experimental one (120 Torr), the effect of pressure variation could be ignored.

4. Conclusions

In the synthesis of diamond/β-SiC nanocomposite films by MWCVD, the possible reactions include Si−C bond breakings in TMS assisted by H/H_2 and successive hydrogen abstraction on SiH_4 and CH_4. The products could be Si, $SiH_n (n = 1-4)$, CH_4, and $(CH_3)_mSiH_n$ ($m = 1-3$, $n = 0-3$, $m + n \leq 4$) species. Due to the smaller ΔE_a values (∼43 kcal/mol) and larger exothermic ΔH_f values (−16.93 to −12.35 kcal/mol) of TMS reactions with H than those with H_2, it is mainly the H radical that causes the Si−C bond breakings in TMS. The rate constants calculated also support such a conclusion. The successive hydrogen abstraction on SiH_4 and CH_4 is the reason why TMS concentration strongly affects the molar fractions of diamond and β-SiC. Because of the low ΔE_a (2−6 kcal/mol) and high exothermic ΔH_f (−36.38 to −15.34 kcal/mol) values, the successive H abstractions from SiH_4 are faster than those from CH_4. The rate constant results by TST also lead to the same conclusion. The overall growth mechanism is highly influenced by the high Si source efficiency facilitated by the presence of TMS with a strong effect on the proportion of diamond and β-SiC in the diamond/β-SiC nanocomposite films deposited by the MWCVD technique.

Acknowledgment. The authors are thankful for the financial support from AvH research foundation and DFG.

References and Notes

(1) Nesladek, M.; Asinari, C.; Spinnewyn, J. *Diamond Relat. Mater.* **1994**, *2*, 7.

(2) Lorenz, H. P. *Diamond Relat. Mater.* **1995**, *4*, 1088.

(3) Fan, Q. H.; Fernandes, A.; Pereira, E.; Gracio, J. *Diamond Relat. Mater.* **1999**, *8*, 1549.

(4) Schaefer, L.; Fryda, M.; Stolley, T.; Xiang, L.; Klages, C.-P. *Surf. Coat. Technol.* **1999**, *116*, 447.

(5) Nono, M. C. A.; Corat, E. J.; Ueda, M. *Surf. Coat. Technol.* **1999**, *112*, 295.

(6) Klages, C.-P.; Fryda, M.; Matthee, T.; Schaefer, L.; Dimigen, H. *Int. J. Refract. Met. Hard Mater.* **1998**, *16*, 171.

(7) *Physics: Theory, and Industrial Practice*; Albright, L. F., Tasi, T. C., Crynes, L. F., Corcoran, W. H., Eds.; Academic: New York, 1983; Chapter 10, pp 233−254.
(8) Konyashin, I. Y.; Guseva, M. B. *Diamond Relat. Mater.* **1996**, *5*, 575.
(9) Glozman, O.; Hoffman, A. *Diamond Relat. Mater.* **1997**, *6*, 796.
(10) Jiang, X.; Klages, C.-P. *Appl. Phys. Lett.* **1992**, *61* (14), 1629.
(11) Jiang, X.; Klages, C.-P. *Diamond Relat. Mater.* **1993**, *2*, 523.
(12) Shi, Y.; Tan, M.; Jiang, X. *J. Mater. Res.* **2002**, *17*, 1241.
(13) Srikanth, Vadali. V. S. S.; Tan, M. H.; Jiang, X. *Appl. Phys. Lett.* **2006**, *88*, 073109.
(14) Seo, Y. H.; Nahma, K. S.; Suh, E.-K.; Lee, H. J.; Hwang, Y. G. *J. Vac. Sci. Technol., A* **1997**, *15* (4), 2226.
(15) Herlin, N.; Lefebvre, M.; Pealat, M.; Perrin, J. *J. Phys. Chem.* **1992**, *96*, 7063.
(16) Avigal, Y.; Schieber, M.; Levin, R. *J. Cryst. Growth* **1974**, *24/25*, 188.
(17) Taylor, J. E.; Milazzo, T. D. *J. Phys. Chem.* **1978**, *82*, 847.
(18) Takahashi, K.; Nishino, S.; Saraie, J. *J. Electrochem. Soc.* **1992**, *139*, 3566.
(19) Lee, Y. L.; Sanchez, J. M. *J. Cryst. Growth* **1997**, *178*, 513.
(20) Henry, F.; Armas, B.; Combescure, C.; Figueras, A.; Garelik, S. *Surf. Coat. Technol.* **1996**, *80*, 134.
(21) Veintemillas, S.; Madigou, V.; Rodriguez-Clemente, R.; Figueras, A. *J. Cryst. Growth* **1995**, *148*, 383.
(22) Ho, P.; Breiland, W. G. *J. Appl. Phys.* **1988**, *63*, 5184.
(23) Frisch, M. J.; Trucks, G. W.; Schlegel, H. B.; Scuseria, G. E.; Robb, M. A.; Cheeseman, J. R.; Zakrzewski, V. G.; Montgomery, J. A. Jr.; Stratmann, R. E.; Burant, J. C.; Dapprich, S.; Millam, J. M.; Daniels, A. D.; Kudin, K. N.; Strain, M. C.; Farkas, O.; Tomasi, J.; Barone, V.; Cossi, M.; Cammi, R.; Mennucci, B.; Pomelli, C.; Adamo, C.; Clifford, S.; Ochterski, J.; Petersson, G. A.; Ayala, P. Y.; Cui, Q.; Morokuma, K.; Malick, D. K.; Rabuck, A. D.; Raghavachari, K.; Foresman, J. B.; Cioslowski, J.; Ortiz, J. V.; Baboul, A. G.; Stefanov, B. B.; Liu, G.; Liashenko, A.; Piskorz, P.; Komaromi, I.; Gomperts, R.; Martin, R. L.; Fox, D. J.; Keith, T.; Al-Laham, M. A.; Peng, C. Y.; Nanayakkara, A.; Gonzalez, C.; Challacombe, M.; Gill, P. M. W.; Johnson, B.; Chen, W.; Wong, M. W.; Andres, J. L.; Gonzalez, C.; Head-Gordon, M.; Replogle, E. S.; Pople, J. A. *Gaussian 03*, Revision B.05; Gaussian, Inc.: Pittsburgh, PA, 2003.
(24) Evans, M. G.; Polanyi, M. *Trans. Faraday Soc.* **1935**, *31*, 875.
(25) Eyring, H. *J. Chem. Phys.* **1935**, *3*, 107.
(26) Steinfeld, J. I.; Francisco, J. S.; Hase, W. L. *Chemical Kinetics and Dynamics*; Prentice Hall: New York, 1998.
(27) Cimalla, V.; Pezold, T. *J. Mater. Res. Soc. Symp. Proc.* **1995**, *355*, 33.
(28) Kordina, O.; Björketun, L. O.; Henry, A.; Hallin, C.; Glass, R. C.; Hultman, L.; Sundgren, J.-E.; Janzen, E. *J. Cryst. Growth* **1995**, *154*, 303.
(29) Roth, P.; Just, Th. *Ber. Bunsen-Ges. Phys. Chem.* **1975**, *79*, 682.
(30) Baulch, D. L.; Cobos, C. J.; Cox, R. A.; Esser, C.; Frank, P.; Just, Th.; Kerr, J. A.; Pilling, M. J.; Troe, J.; Walker, R. W.; Warnatz, J. *J. Phys. Chem. Ref. Data* **1992**, *21*, 411.
(31) Frank, P. *Proc. Int. Symp. Rarefied Gas Dyn.* **1986**, *2*, 422.